Cancer Management and Research

Dovepress
open access to scientific and medical research

Open Access Full Text Article

ORIGINAL RESEARCH

Magnetic Resonance Diffusion Kurtosis Imaging versus Diffusion-Weighted Imaging in Evaluating the Pathological Grade of Hepatocellular Carcinoma

This article was published in the following Dove Press journal:
Cancer Management and Research

Guang-Zhi Wang[1,2]
Ling-Fei Guo[3]
Gui-Hua Gao[3]
Yao Li[4]
Xi-Zhen Wang[2]
Zhen-Guo Yuan[1,3]

[1]Cheeloo College of Medicine, Shandong University, Jinan 250021, People's Republic of China; [2]Department of Medical Imaging Center, Affiliated Hospital, Weifang Medical University, Weifang 261053, People's Republic of China; [3]Department of MRI, Shandong Medical Imaging Research Institute, Cheeloo College of Medicine, Shandong University, Jinan 250021, People's Republic of China; [4]Zhucheng People's Hospital Affiliated to Weifang Medical University, Weifang 262200, People's Republic of China

Purpose: To investigate the diagnostic efficacy of diffusion kurtosis imaging (DKI) and conventional diffusion-weighted imaging (DWI) for pathological grading.

Methods: From December 2015 to January 2017, consecutive patients suspected of having hepatocellular carcinoma (HCC) without prior treatment were prospectively enrolled in this study. MRI examinations were performed before surgical treatment. HCC patients confirmed by surgical pathology were included in the study. The mean diffusivity (MD) values, mean kurtosis (MK) values, and apparent diffusion coefficient (ADC) were calculated. The differences and correlations of these parameters among different pathological grades were analyzed. The diagnostic efficiency of DKI and DWI for predicting high-grade HCC was evaluated by receiver operating characteristic (ROC) curves. Logistic regression analyses were used to evaluate the predictive factors for pathological grade.

Results: A total of 128 patients (79 males and 49 females, age: 56.9±10.9 years, range, 32–80) with primary HCC were included: grade I: 22 (17.2%) patients, grade II: 37 (28.9%) patients, grade III: 43 (33.6%) patients, grade IV: 26 (20.3%) patients. The MK values of stage I, II, III, and IV were 0.86±0.13, 1.06±0.11, 1.27±0.17, and 1.57±0.13, respectively. The MK values were significantly higher in the high-grade group than in the low-grade group and were positively correlated with pathological grade (*rho* =0.7417, $P<0.001$). The MK value demonstrated a larger area under the curve (AUC), with a value of 0.93 than the MD value, which had an AUC of 0.815 ($P<0.001$), and ADC, which had an AUC of 0.662 ($P=0.01$). The MK value (>1.19), ADC ($\leq 1.29\times10^{-3}$ mm^2/s), and HBV (+) were independent predictors for the pathological grade of HCCs.

Conclusion: The MK values derived from DKI and the ADC values obtained from traditional DWI were more valuable than the MD values in predicting the histological grade of HCCs and could potentially guide clinical treatment before surgery.

Keywords: hepatocellular carcinoma, pathology, diffusion kurtosis imaging, diffusion-weighted imaging, predictor

Introduction

Hepatocellular carcinoma (HCC) is the fifth most common cancer and the second most frequent cause of cancer-related death worldwide.[1] Previous studies have suggested that the differentiation of HCC could affect the recurrence rate and disease-free survival after resection or liver transplant, and a higher pathological grade is associated with worse prognosis.[2,3] Thus, an accurate pathological grading

Correspondence: Zhen-Guo Yuan
Shandong Medical Imaging Research Institute, Cheeloo College of Medicine, Shandong University, No. 324, Jing-wu road, Huaiyin District, Jinan 250021, People's Republic of China
Email yuanzg88@126.com

submit your manuscript | www.dovepress.com
DovePress
http://doi.org/10.2147/CMAR.S254371

method for HCC could help guide the selection of a treatment strategy, which can be implemented to improve the treatment effects as well as to prolong patient survival.[4] In clinical practice, the pathological grade is routinely determined after resection. Although puncture biopsy can help to diagnosis, unfortunately, this method is invasive and limited in HCC pathological grading. Because some components with different histological grades are often included in an HCC nodule, a noninvasive method that can preoperatively reflect the overall tissue condition of the tumor is needed.[5]

Computed tomography (CT) and magnetic resonance imaging (MRI) are the most commonly used non-invasive evaluation tools in the diagnosis and treatment of HCC and can provide useful pathological information.[6–8] Some studies have already reported evaluating tumor histological grade using diffusion-weighted imaging (DWI), but this functional MR imaging technique only reveals the Gaussian water diffusivity.[9,10] The recently developed diffusion kurtosis imaging (DKI) technique is based on the localized in vivo non-Gaussian diffusion of water molecules resulting from the structural and morphological complexity of the tissues (e.g., the intrinsic biochemical properties of different types of cells and tissues), which was first proposed by Jensen in 2005.[11,12] Compared to normal diffusion in the tissue, non-Gaussian diffusion has higher peak values. DKI can quantify the actual diffusion of water molecules and the degree of displacement from an ideal Gaussian distribution. In other words, DKI is mainly employed to detect the properties of non-Gaussian water molecules diffusion in tissues, and the results reflect the microstructural complexity of the tissue.[9,13,14] The most representative parameter of DKI is mean kurtosis (MK), which is considered an indicator of the complexity of the tissue microstructure; MK is a dimensionless parameter that reflects the restriction of the degree of diffusion. The intensity of MK depends on the complexity of the tissue structure with significantly more restricted non-Gaussian diffusion in tumors. Mean diffusion diffusivity (MD) represents the non-Gaussian distribution corrected by the average apparent diffusion coefficient (ADC); this value reflects only the diffusion of water molecules. Currently, DKI has been used in the evaluation of many diseases, such as kidney and prostate malignancies,[15–17] and has shown a better performance for characterizing and grading tumors than conventional DWI.[18] Additionally, DKI typically can accurately describe the diffusion information and reflect the microstructure of the tissue.[19] However, there have been few studies on the application of DKI in the pathological grading of HCC, and the results were variable and inconsistent.[20,21]

In this study, we prospectively investigated the features of the functional parameters derived by conventional DWI and DKI for HCC with different pathological graded and evaluated the diagnostic efficacy of DKI in the pathological grading of HCC.

Methods

Patients

This study received approval from the Institutional Review Board of Weifang Medical University Affiliated Hospital and complied with the Declaration of Helsinki. Written informed consent was provided by all subjects. From December 2015 to January 2017, consecutive patients suspected of having HCC or focal hepatic lesions based on the clinical history or previously performed sonography or CT were subjected to MRI examinations (including routine plain scans, dynamic enhanced scans, DKI, and DWI sequences) before surgical treatment. The inclusion criteria include: (1) histologically confirmed HCC without prior treatment; (2) surgical resection performed within 14 days after MRI examination; (3) solitary lesion, or ≤5 multiple HCCs; (4) maximal lesion diameter <10; and (5) history, physical examination, laboratory measurements, imaging data and treatment strategies were recorded in detail. The exclusion criteria include (1) non-HCC confirmed by biopsy or post-surgical pathological results; (2) patients with contraindication for MRI; and old age or patients in severe conditions who could not follow respiratory exercises, which caused artifacts on the images; (3) lesions less than 1 cm in diameter, for which the ROI could not be precisely obtained; (4) >5multiple HCCs or diffuse HCCs; and (5) patients with active hepatitis upon whom surgery cannot be performed.

All patient' history, physical examinations, and laboratory examinations were recorded before surgery, which include routine blood tests, liver function and alpha fetal protein (AFP) levels, tumor status, Eastern Cooperative Oncology Group Performance Score, Barcelona Clinic Liver Cancer (BCLC) stage and Child–Pugh score.[22] AFP levels >400 μg/L were considered high-concentration positives (the normal value ranged from 0 to 25 μg/L).

MRI Examination

Instruments and Body Position

All patients were examined using a 3.0T MR scanner (MAGNETOM Skyra, Siemens Healthcare, Erlangen, Germany) with an 18-channel phased-array body coil. All patients fasted for 6–8 hours prior to the examination, and all received training to perform even breathing and breath-holding.

Scanning

The MRI protocols included transverse fat-suppressed T_2-weighted imaging (T_2WI), T_1- weighted imaging (T_1WI), a coronal T_2WI-half-Fourier acquisition single-shot turbo spin-echo (T_2WI-HASTE) sequence, a transverse DWI sequence, a transverse T_1 in- and out-of-phase sequence, a transverse T_1-VIBE sequence, and DKI sequence. The scan range extended from the top of the diaphragm to the lower end of the liver. A single-shot echo-planar DWI pulse sequence was employed to acquire the DKI data. The parameters were as follows: repetition time (TR) = 3300 ms, echo time (TE) = 88 ms, flip angle (FA) = 90°, slice thickness = 5 mm with a slice gap of 1.5 mm, field of view (FOV) = 380×420 mm^2, matrix size = 168×105, and acquisition time = 5 min. Three b values of 0, 800, and 1500 s/mm^2 were applied in at least 3 gradient directions.[9,23]

Three-Phase Dynamic-Contrast Enhanced (DCE) MRI of the Liver

The contrast agent Gadolinium-diethylene triamine pentaacetic acid (Gd-DTPA) (Omniscan, GE Healthcare) was injected using a high-pressure injector at a flow rate of 3 mL/s and a dosage of 0.2 mmol/kg per weight. A 20-mL saline bolus was injected at the same flow rate immediately after the contrast agent injection. The arterial phase scan started 15 s after the contrast agent injection (15 s is the time needed for the contrast agent to reach the upper abdomen).[24] This examination included a transverse liver artery phase, portal venous phase (scan started 55 s after the contrast agent injection), delayed phase T_1WI (scan started 1 min and 25 s after the contrast agent injection), and coronal and sagittal enhanced T_1WI.

Image Processing and Analysis

All data obtained by DWI and DKI were analyzed using publicly available postprocessing software (DKE, Medical University of South Carolina, Charleston, USA). According to the DKI model,[25–27] $S=S_0\cdot\exp(-b\cdot D+b^2\cdot D^2\cdot K/6)$, where b represents the b-value, D represents the corrected apparent diffusion accounting for non-Gaussian diffusion behavior, and K represents apparent kurtosis coefficient (the deviation of tissue diffusion from a Gaussian distribution).[28] The software also calculated the ADC using b-values = 0 and 800 s/mm^2 based on a monoexponential model: $S=S_0\cdot\exp(-b\cdot ADC)$. Based on these calculations, the D, K, and ADC maps were obtained.[29,30] ROIs were manually drawn on solid parts of the largest lesions by two independent senior radiologists (Z.G.Y. and Y.L., with more than 10 years of experience in abdominal imaging) who were blinded to the clinical and pathological results. Care was taken to avoid large vessels, bile ducts, necrosis and artifacts. Finally, the MK, MD and ADC values were obtained. The general potential predictive features, including tumor size, number of lesions, signal homogeneity on T_2WI, tumor margin, radiologic capsule, peripheral enhancement during the arterial phase, satellite nodules, intratumor fat deposition, vascular invasion, and enhancement pattern were also assessed on conventional T_1-weighted, T_2-weighted and contrast-enhanced MR images.[20,31] When there was a discrepancy between the two reviewers' findings, a joint review was performed, and the consensus was used for the statistical analysis.

Pathological Examination

The surgically removed resected hepatic specimens were fixed with formalin. The tissues were dehydrated following the regular procedure, embedded in paraffin, and sectioned. Hematoxylin and eosin (H&E) and immunohistochemical staining protocols were performed. All pathological specimens were reviewed by a pathologist (with 20 years of experience in liver pathology). The pathological grade of HCC was determined according to the Edmondson-Steiner classification.[32] Tumors classified as Edmondson–Steiner grades I and II were included in the low-grade group, and those classified grades III and IV were included in the high-grade group.

Statistical Analysis

Continuous variables are expressed as means ± standard deviations or medians, and categorical variables were presented as frequencies and percentages. The interobserver reproducibility of continuous variables between two independent radiologists was evaluated using the mean difference with 95% limits of agreement (LoA) and Bland–Altman plots.[33] If the results between the two readers were

Table 1 Baseline Clinical Characteristics of the Patients Before Surgery (n=128)

Characteristics	N (%)
Age, years	56.9±10.9
Range	32.0–80.0
Gender	
Male	79 (61.7%)
Female	49 (38.3%)
Hepatitis	
Negative	39 (30.5%)
HBV (+)	83 (64.8%)
HCV (+)	6 (4.7%)
ECOG performance status	
PS 0	99 (77.3%)
PS 1	21 (16.4%)
PS 2	8 (6.2%)
Child–Pugh	
A	100 (78.1%)
B	28 (21.9%)
Serum AFP level	
<400 ng/mL	86 (67.2%)
≥400 ng/mL	42 (32.8%)
Number of tumors	
Solitary	116 (90.6%)
Multiple	12 (9.4%)
Size of tumor	8.4 (± 3.9)
≤5 cm	36(28%))
5–10 cm	51(40%)
>10 cm	41(32%)
BCLC stage	
A	81 (63.3%)
B	18 (14.1%)
C	29 (22.7%)

Abbreviations: ECOG, Eastern Cooperative Oncology Group; AFP, alpha fetal protein; BCLC, Barcelona Clinic Liver Cancer.

consistent, the parameters of one radiologist were used for analysis. One-way ANOVA or the Kruskal–Wallis rank test was used to compare the differences in DKI/DWI parameters and pathological grades. Spearman correlation analysis was implemented to determine the degree of correlation between the corresponding parameters and pathological grade, and each result obtained is expressed as the correlation coefficients (*rho*).[33] Univariate and multivariate binary logistic regression analyses were used to identify independent predictors of pathological grades. Odds ratios (ORs) and 95% confidence intervals (CIs) were calculated.[20] Receiver operating characteristic (ROC) analyses were performed to evaluate the diagnostic performance of significant parameters in predicting high-grade HCC. The optimal cut-off point that demonstrated the greatest Youden index and the corresponding sensitivity, specificity, and positive and negative likelihood ratio was calculated.[34] The Bland–Altman test was performed using MedCalc (MedCalc Software, Ostend, Belgium), and the other statistical analyses were performed using SPSS 20.0 statistical software (IBM, New York). P <0.05 was considered statistically significant.

Results

Clinical Characteristics of the Patients

A total of 128 patients who satisfied the inclusion criteria and underwent various examinations were included. Among them, 49 were male, and 79 were female. The average patient age was 56.9±10.9 years (ranging from 32 to 50, median age: 58). A total of 16 patients with no apparent symptoms were found to have with space-occupying lesions during physical exams. A total of 97 patients experienced abdominal distension or discomfort, 11 patients experienced weight loss and jaundice, and 3 patients had abdominal pain and hematemesis. The laboratory examination results were as follows: 83 (64.8%) patients were hepatitis B surface antigen (HBsAg) positive (HBV(+)), 6 were hepatitis C infection positive (HCV(+)), and 39 (30.5%) were negative; 42 patients (32.8%) showed AFP levels ≥400 ng/mL. A total of 100 (78.1%) patients were classified as Child–Pugh grade A. The patient characteristics are summarized in Table 1.

Conventional MR Imaging and Pathologic Findings

The median interval between MRI and resection was 6 days (ranging from 1 to 14). Among the 128 HCC patients, 12 (9.4%) had multiple lesions, and 116 (90.6%) had solitary lesions. All lesions were in the right lobe of the liver. The maximum tumor diameter was 8.4 ± 3.9 cm (ranging from 3.0 to 18.0 cm). The tumors had low or slightly low T_1WI signals and higher T_2WI signals. The signals of larger-volume tumors, necrotic tumors, or cystic tumors were more complicated. In the arterial phase after the injection of Gd-DTPA, weak enhancement was observed in 6 cases, weak-medium enhancement was observed in 10 cases, medium enhancement was seen in 23 cases, and strong enhancement was seen in 89 cases. Homogenous enhancement was observed in 36 cases,

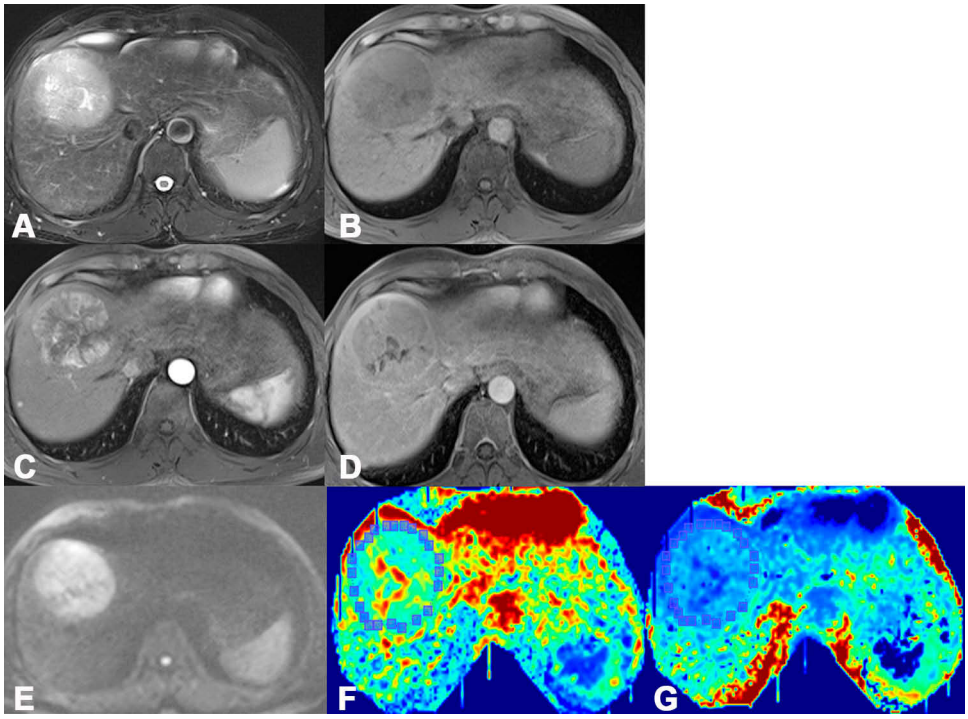

Figure 1 One case of an HCC patient, male, age 52 years, hepatitis B (+). High MRI FS-T2 WI signal (**A**), low T1 WI signal (**B**), apparent enhancement of lesions in the arterial phase (**C**), and reduced enhancement in the venous phase (**D**). Figures (**E**), (**F**), and (**G**) are images based on the parameters ADC, MK, and MD.

while 92 cases showed heterogeneous enhancement (Figure 1). According to the Edmondson-Steiner classification, 22 (17.2%) cases were stage I, 37 (28.9%) cases were stage II, 43 (33.6%) cases were stage III, and 26 (20.3%) cases were stage IV. A total of 59 cases were classified as the low-grade group (I+II), while 69 were classified as the high-grade group (III+IV). Among the MR imaging features, the number of lesions, signal homogeneity, tumor margin, radiologic capsule, peripheral enhancement, intratumor fat deposition, satellite nodules, and enhancement pattern were not significantly different between the low- and high-grade groups. The tumor size and degree of vascular invasion, however, were significantly greater in the high-grade group than in the low-grade group (P = 0.0007 and 0.0021, respectively) (Table 2).

Relationship Between DKI and ADC Parameters versus Pathological Grade

The ADC, MK, and MD values obtained from postprocessed DKI-DWI sequences were subjected to statistical analysis referencing the different pathological grades of HCC patients. The mean absolute differences in ADC, MK, and MD values between the two radiologists were 0.015 $\times 10^{-3}$ mm^2/s (LOA −0.302–0.271), 0.004 (LOA −0.332–0.323), and 0.008 mm^2/s (LOA −0.246–0.230), respectively (Figure 2). The reproducibility of all ADC and DKI parameters was better than that of DWI parameter, all of which are displayed in Table 3. Significant differences were observed in ADC, MK, and MD values among pathological grades I, II, III, and IV (P<0.001). The MK values for stages I, II, III, and IV were 0.86±0.13, 1.06±0.11, 1.27±0.17, and 1.57±0.13, respectively. As the decrease in pathological grade decreased, the MK value significantly increased, whereas the MD value obtained by DKI and ADC value obtained by traditional DWI significantly decreased as the pathological grade increased (Table 4). The MK values were significantly higher in the high-grade group than in the low-grade group and were positively correlated with pathological grade (rho =0.7417, P<0.001). The ADC and MD values were all negatively correlated with pathological grade (rho = –0.5436, rho = –0.2806, P<0.001, respectively) (Table 3). The violin plots of the ADC, MK and MD values versus HCC pathological grade are shown in Figure 3.

In discriminating low-/high-grade HCCs, MK demonstrated a larger area under the curve (AUC), with a value of 0.93 (95% CI, 0.870–0.967), than ADC, which had an AUC of 0.815 (95% CI, 0.737–-0.878, P<0.001), or MD, which had an AUC of 0.662 (95% CI, 0.574–0.744, P=0.01). The optimal MK cutoff

Table 2 Radiologic Features of Low- and High-Grade HCCs

	Overall (N=128)	Low-Grade (N=59)	High-Grade (N=69)	*P*
Tumor size		7.15±3.71	9.55±3.80	0.0007
Signal homogeneity				0.5933
Homogenous	22 (17.2)	9 (15.3)	13 (18.8)	
Heterogeneous	106 (82.8)	50 (84.7)	56 (81.2)	
Tumor margin				0.0540
Irregular	37 (28.9)	22 (37.3)	15 (21.7)	
Smooth	91 (71.1)	37 (62.7)	54 (78.3)	
Radiologic capsule				0.4651
Absent	52 (40.6)	26 (44.1)	26 (37.7)	
Present	76 (59.4)	33 (55.9)	43 (62.3)	
Peripheral enhancement				0.3104
Absent	83 (64.8)	41 (69.5)	42 (60.9)	
Present	45 (35.2)	18 (30.5)	27 (39.1)	
Satellite nodules				0.1400
Absent	111 (86.7%)	54 (91.5%)	57 (82.6%)	
Present	17 (13.3%)	5 (8.5%)	12 (17.4%)	
Fat deposition				0.1809
Absent	92 (71.9)	39 (66.1)	53 (76.8)	
Present	36 (28.1)	20 (33.9)	16 (23.2)	
Vascular invasion				0.0021
Absent	84 (65.6%)	47 (79.7%)	37 (53.6%)	
Present	44 (34.4%)	12 (20.3%)	32 (46.4%)	
Enhancement pattern				0.2404
Typical	41 (32.0)	22 (37.3)	19 (27.5)	
Typical	87 (68.0)	37 (62.7)	50 (72.5)	

value was 1.19 and the sensitivity, specificity, and Youden index of MK in predicting high-grade HCC were 78.26%, 94.92% and 0.73, respectively (Table 5). The optimal MD and ADC cutoff values were 0.70×10^{-3} mm^2/s and 1.29×10^{-3} mm^2/s, respectively (Figure 4).

Predictors for the Pathological Grade of HCC

Hepatitis B virus (+), serum AFP level, tumor number, tumor size, BCLC stage B/C, ADC ($\leq1.29\times10^{-3}$ mm^2/s), MK ($>1.19\times10^{-3}$ mm^2/s) and MD ($\leq0.70\times10^{-3}$ mm^2/s) were identified as independent predictors of high grade of HCCs in univariate logistic analysis (Table 6). In multivariate analysis, only the MK value ($>1.19\times10^{-3}$ mm^2/s) [OR: 0.015 (95% CI, 0.001–0.174), P=0.001], ADC value ($\leq1.29\times10^{-3}$ mm^2/s) [OR: 0.007 (95% CI, 0.001–0.066), <0.001] and HBV (+) [OR: 0.089 (95% CI, 0.017–0.477), P=0.005] were identified as independent predictors for pathological grading of HCCs.

Discussion

We evaluated the application of DKI in the pathological grading of HCCs in this study. DKI acquisition and analysis were successfully performed for all patients. Rosenkrantz et al exploited the ADC and DKI parameters for a preliminary study on fresh liver explants in patients with hepatocellular carcinoma and demonstrated that the ADC, MD, and MK values were useful for the determination of liver partial necrosis, complete necrosis, and response to treatment.[29] Other studies identified MK and MD values for staging hepatic fibrosis.[35,36] In this study, the MK and MD values obtained by DKI were significantly correlated with the pathological grade of HCC. We also found that the general features, including tumor size and vascular invasion, were significantly greater in the high-grade group than in the low-grade group, and were significantly related to high-grade HCCs by univariate analysis; however, only the MK value ($>1.19\times10^{-3}$ mm^2/s), ADC value ($\leq1.29\times10^{-3}$ mm^2/s) and HBV (+) were identified as independent predictors for pathological grading of HCCs in multivariate analyses. The results in other studies differed to varying degrees,[20,31,37] which may be caused by bias in selecting patients or surgical candidates among different studies.

The MK values showed a statistical difference from the MD and ADC values in predicting the histological grade of HCCs, which was similar to previous studies.[20,21,38] The kurtosis of tissues based on a non-Gaussian distribution was influenced by the higher tissue complexity and heterogeneity. Because vigorous cell proliferation, a more tortuous extracellular space, inflammation, necrosis and hemorrhage are more common in high-grade HCCs, a more peaked distribution of tissue diffusivities is likely to occur.[20,21] Kurtosis also partially represents the interaction of water molecules with cell membranes and intracellular compounds.[10,20] The irregular distribution of tumor cells and heterogeneous extracellular medium results in a marked hindrance of water motion and interactions with the cell membranes.[39] Therefore, the MK values increased as the HCC pathological grade increased from stage I to IV, and a good correlation was shown between

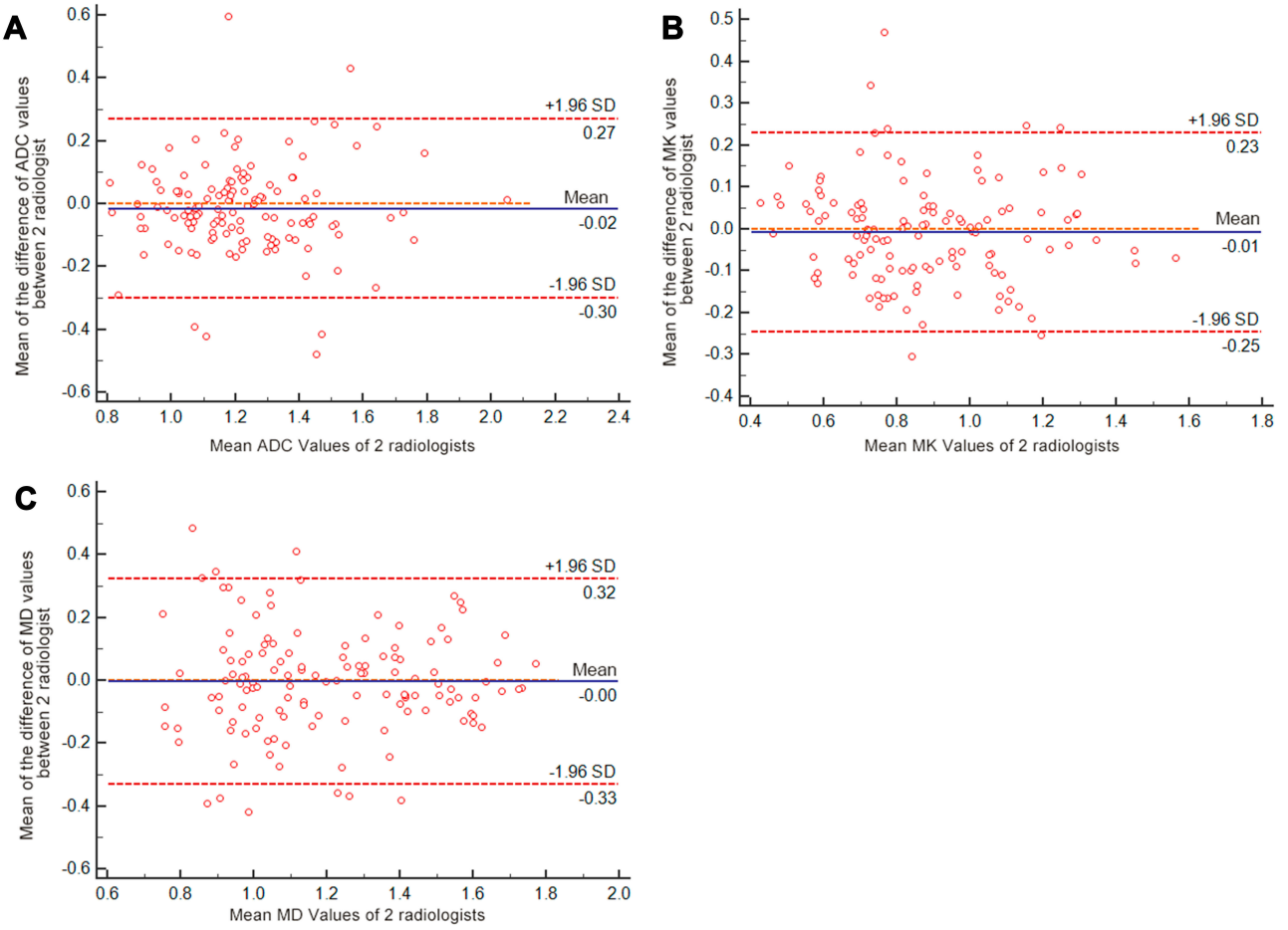

Figure 2 Bland–Altman plots showing the reproducibility of ADC MK and MD values between the two observers. (**A**) The mean difference in ADC values between the two radiologists was 0.015 $\times 10^{-3}$ mm^2/s (LOA −0.302–0.271), the mean difference in MK values was 0.004 (LOA −0.332–0.323) (**B**), and the mean difference in MD values was 0.008 mm^2/s (LOA −0.246–0.230) (**C**). The blue line represented the mean difference between two observers, red lines represented the 95% confidence interval of the mean difference (limits of agreement, LOAs).

Table 3 Correlations Between DKI/DWI Parameters and HCC Pathological Grades Evaluated by Each Radiologist

Parameters	Radiologist 1				Radiologist 2			
	Low-Grade	High-Grade	*P*	*rho*	Low-Grade	High-Grade	*P*	*rho*
ADC ($\times 10^{-3}$ mm^2/s)	1.35±0.25	1.10±0.14	<0.001	−0.5436**	1.34±0.25	1.14±0.16	<0.001	−0.4392**
MK	0.99±0.15	1.38±0.22	<0.001	0.7417**	0.97±0.14	1.40±0.20	<0.001	0.7905**
MD ($\times 10^{-3}$ mm^2/s)	0.95±0.24	0.81±0.22	0.001	−0.2806**	0.96±0.24	0.82±0.23	0.0009	−0.278**

Note: **P value <0.01.

Table 4 Parameters of DKI and DWI in Different HCC Pathological Grades

Parameters	Grade I	Grade II	Grade III	Grade IV	*P*	*rho*
ADC($\times 10^{-3}$ mm^2/s)	1.46±0.31	1.28±0.18	1.13±0.12	1.05±0.14	<0.001	−0.5727**
MK	0.86±0.13	1.06±0.11	1.27±0.17	1.57±0.13	<0.001	0.8499**
MD($\times 10^{-3}$ mm^2/s)	1.07±0.25	0.87±0.20	0.91±0.19	0.66±0.15	<0.001	−0.4732**

Note: **P value <0.01.

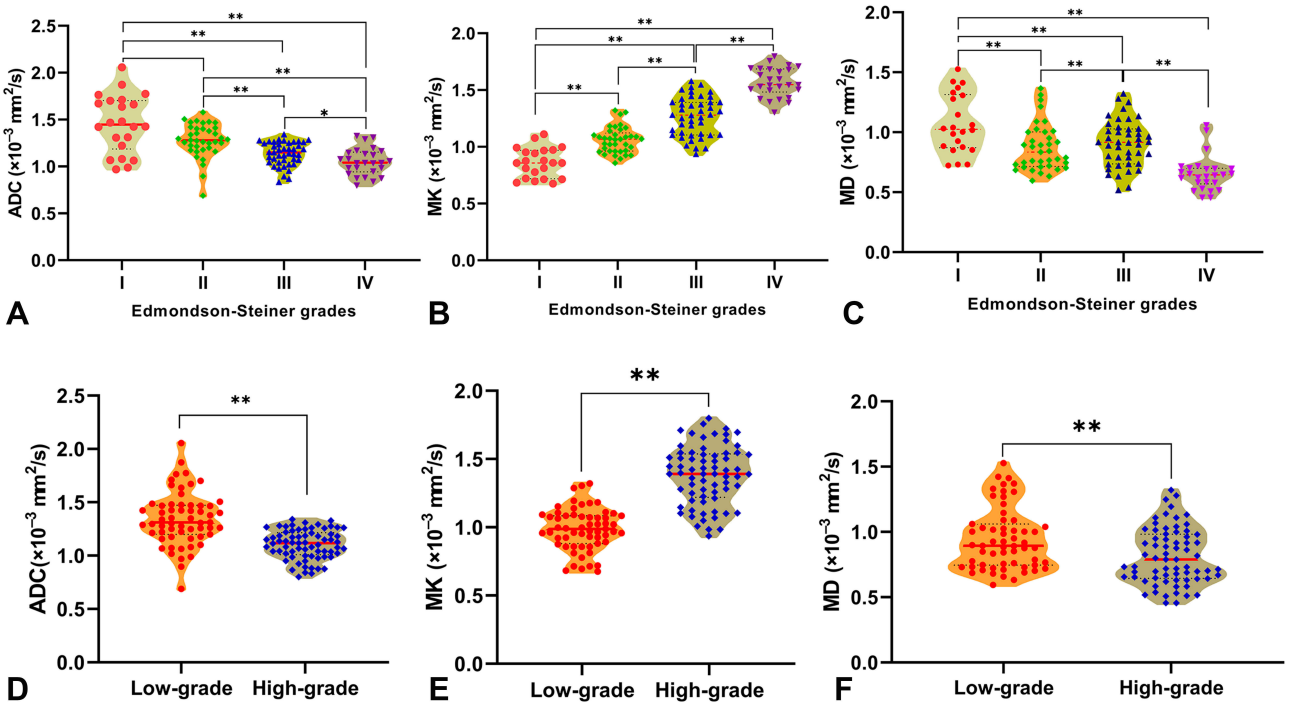

Figure 3 The Violin plots of the ADC, MK and MD values classified by HCC pathological grade. Significant differences were observed in ADC (**A**), MK (**B**) and MD (**C**) values among different pathological grades I, II, III, and IV. The differences in ADC (**D**), MK (**E**) and MD (**F**) values between low- and high-grade HCC were also statistically significant (**P<0.001; *P<0.05).

MK and pathological grade (*rho*=0.8499). Thus, the MK value, as the most significant parameter, allows for the preliminary preoperation pathological grading for HCC patients.

The MD value obtained from DKI was similar to the ADC value obtained from DWI. These parameters depend mainly on the diffusion of water molecules in tissue, which is restricted when pathological changes lead to high cell density and a narrow extracellular space. In HCC tissue, the cells were more tightly aligned, the volume of the cell nucleus was increased, and the intercellular cavity space decreased the exuberant cell proliferation. This resulted in the restricted diffusion of water molecules, which presented as decreased ADC and MD values. Therefore, the MD and ADC values decreased as the HCC pathological grade increased, and negatively correlated with the pathological grade in our study. This means that the degree of restriction on diffusion for HCC with low-differentiated (stages III and IV) was more obvious than that for HCC with medium-to-high differentiation (stages I and II), and the MD values for HCC with low differentiation were lower than those for HCC with medium-to-high-differentiation.

However, the correlation between the MD value and HCC pathology (rho= −0.4732) was worse than that between the ADC value and HCC pathology (rho= −0.5727) in our study. This discrepancy is likely to be attributed to the selection of b-values. The regular DWI sequence only requires two b values to generate an ADC map. With the high b-values in our study, the ADC value influenced by microcapillary perfusion might be reduced, and can truly reflect water diffusion, but requires an obviously prolonged scan time and has a reduced

Table 5 Diagnostic Efficacy of DKI Evaluated by Receiver Operating Characteristic Analysis

	Cut-Off	Sensitivity	95% CI	Specificity	95% CI	Youden	AUC	95% CI
ADC	≤1.29	94.2%	85.8–98.4	57.63%	44.1–70.4	0.52	0.815	0.737–0.878
MK	>1.19	78.26%	66.7–87.3	94.92%	85.9–98.9	0.73	0.93	0.870–0.967
MD	≤0.70	39.13%	27.6–51.6	89.83%	79.2–96.2	0.29	0.662	0.574–0.744

Abbreviations: CI, confidence interval; AUC, area under the receiver operating characteristic curve.

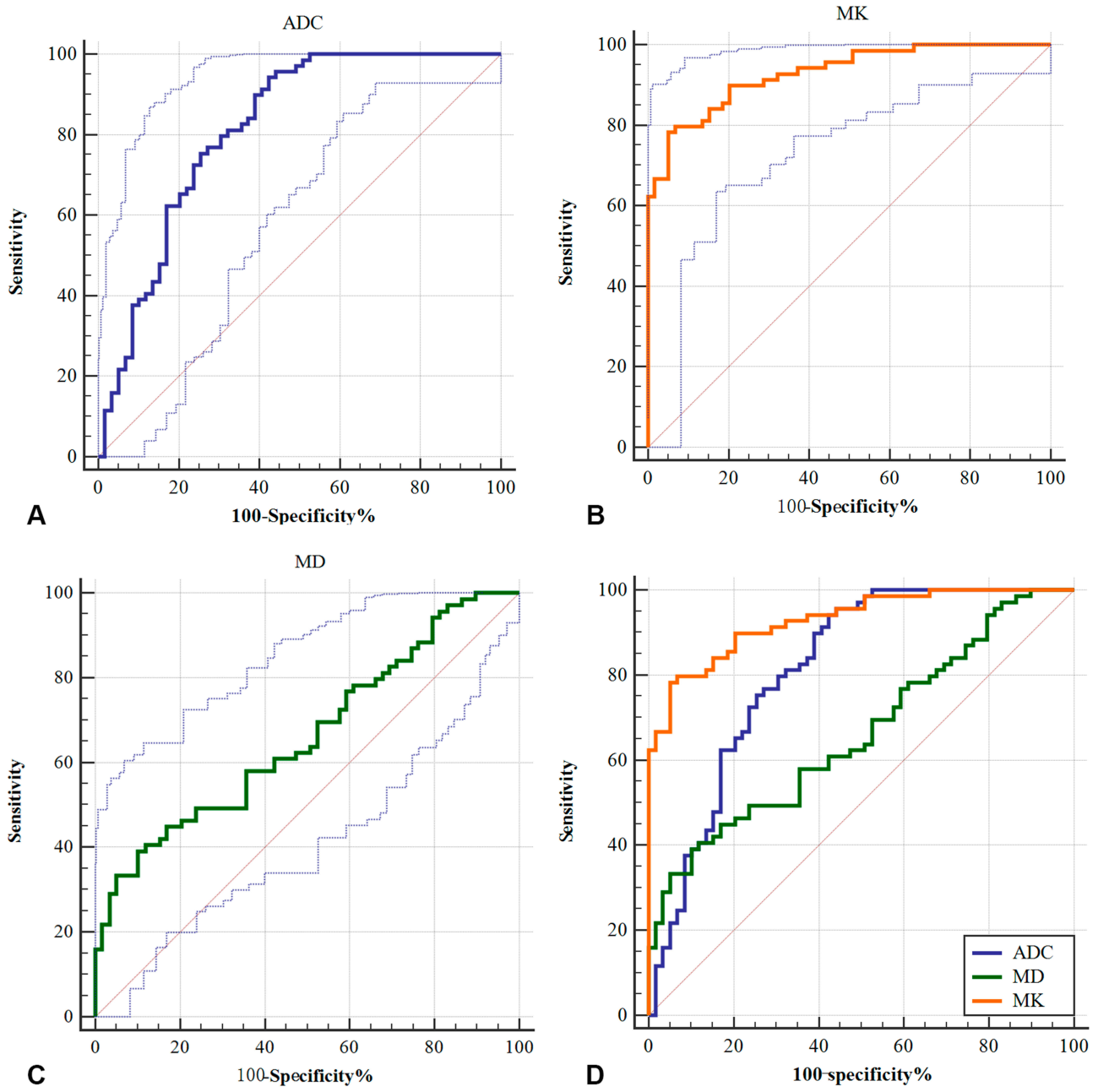

Figure 4 Receiver operating characteristic (ROC) curves of ADC, MK and MD values for discriminating low-/high-grade HCC. (**A**) The area under the curve (AUC) of the ADC value was 0.662 (95% CI, 0.574–0.744), with an optimal cutoff value of 1.29×10^{-3} mm^2/s; (**B**) the AUC of the MK values was 0.93 (95% CI, 0.870–0.967), with an optimal cutoff value of 1.19; (**C**) the AUC of the MD values was 0.815 (95% CI, 0.737–0.878), with an optimal cutoff value of 0.70×10^{-3} mm^2/s; (**D**) the AUCs of the MK, MD and ADC values were statistically significant from one another ($P<0.001$).

signal-to-noise ratio. On the other hand, with a lower b value, the ADC values can be influenced by blood perfusion.[40] Most studies have considered that the appropriate b value should be 400–800 s/mm^2 for hepatic DWI imaging.[34,41] In our study, two b values were selected for traditional DWI: 0 and 800 s/mm^2. However, DKI sequences require multi-b values and a high b value is needed for non-Gaussian computational model fitting and to obtain parameters such as Kapp. Studies on the applications of the DKI technique have mostly exploited parameters such as MD and MK calculated using high b values. In studies of brain DKI, the maximum b value should be 2000–3000 s/mm^2.[2,42,43] However, in the applications of DKI for abdominal examinations, excessively high b values for imaging should be avoided.[28] As the b values increase, the requirements for the scanning instrument become higher, the scan time becomes longer, and the signal intensity and the T_2

Table 6 Univariate and Multivariate Analysis of Predictors of HCC Pathological Grade

Factors	Univariate Analysis		Multivariate Analysis	
	OR(95% CI)	***P***	**OR(95% CI)**	***P***
Age (y)	1.101(0.969–1.033)	0.959		
Gender	0.707(0.344–1.454)	0.346		
HBV(+)	0.096(0.040–0.230)	<0.001**	0.089(0.017–0.477)	0.005*
ECOG		0.179		
PS 0				
PS 1	0.327(0.063–1.698)	0.183		
PS 2	0.667(0.106–4.196)	0.666		
Child–Pugh A-B	0.578(0.243–1.376)	0.215		
AFP level	1.032(1.017–1.046)	<0.001**		
Tumor number	0.207(0.043–0.986)	0.048*		
Tumor size	1.185(1.072–1.310)	0.001*		
BCLC stage		0.007*		
A				
B	4.600(1.392–15.196)	0.012*		
C	2.921(1.186–7.192)	0.020*		
Vascular invasion	0.295(0.134–0.651)	0.03*		
ADC values	0.045(0.015–0.141)	<0.001**	0.015(0.001–0.174)	0.001**
MK values	0.020(0.006–0.065)	<0.001**	0.007(0.001–0.066)	<0.001**
MD values	0.176(0.067–0.466)	<0.001**		

Notes: *P value <0.005; **P value <0.01.

WI signal decreases more rapidly, which severely affects the signal-to-noise ratio of the images and impedes the postprocessing. Therefore, it is unnecessary to apply excessively high b values. Moreover, at smaller b values, the signals gained from the non-Gaussian diffusion model are weaker, and the slope deviation from the Gaussian distribution cannot be detected. Thus, an appropriate b value is needed. According to recent studies on the application of DKI in abdominal examinations,[19,38,44,45] non-Gaussian models perform better when the maximum b value is in the 1500–2000 s/mm^2 range. In our study, we selected three b values for DKI: 0, 800, and 1500 s/mm^2. Jensen et al reported that the MK and MD values can be acquired using at least 3 gradient directions when performing DKI of the abdomen.[46] Budjan et al considered that the assessment of conventional ADC values leads to similar results when using b-values below 1000 s/mm^2 for the MD analysis. This might explain the lack of association between MD and ADC values and HCC pathological grade in this study.

There were several limitations in our study. First, the sample size was relatively small for multivariate analysis. However, these results were consistent with the results of other studies, and the sample size was larger than these similar studies.[20,34] Second, the DKI technical parameters, especially b values setting, are crucial for accurate quantitation of tissue diffusion. However, no standardized protocol regarding the proper b values and settings of some other imaging parameters has been established so far, and the results vary greatly among different studies. When applying DKI to abdominal examinations, the b value is typically 1800 or 2000 s/mm^2. However, we selected three b values for DKI: 0, 800, and 1500 s/mm^2 to balance the image quality and accuracy of the parameters. Third, artifacts caused by breathing, bowel movements, and other factors such as uneven coil for the abdomen can cause reductions in image quality and the signal-to-noise ratio. Additionally, HCCs typically develop from liver cirrhosis. At the late stage of liver cirrhosis, portal hypertension and ascites are observed, which can lead to severe artifacts on DKI images. These artifacts can seriously influence the measurement of the parameters during image post-processing. A reduction in echo time using respiratory-triggered and artifact removal techniques could

be achieved to remove artifacts and improve image quality in the future. Therefore, the applicability of DKI parameters in HCC pathological grading should be further confirmed.

Conclusion

The MK values obtained from DKI, combination with the ADC value obtained from traditional DWI, more valuable for predicting the histological grade of HCCs than the MD values. The DKI technique is potentially applicable in the preoperation evaluation of HCC grade and can provide an excellent reference for guiding the clinical treatment of HCC patients.

Funding

This study was supported by grants from Shandong Province Science and Technology Development Project [grant number 2012YD18064], Project of Medicine and Health Development Plan of Shandong Province [grant number 2011HW067], Shandong Provincial Natural Science Foundation [grant number ZR2013HM071], and Key Research and Development Program of Shandong Province [grant number GG2018G SF118171].

Disclosure

The authors declare that there are no conflicts of interest.

References

1. Siegel RL, Miller KD, Jemal A. Cancer statistics, 2020. *CA Cancer J Clin*. 2020;70:7–30. doi:10.3322/caac.21590
2. Tamura S, Kato T, Berho M, et al. Impact of histological grade of hepatocellular carcinoma on the outcome of liver transplantation. *Arch Surg*. 2001;136:25–30;discussion 31. doi:10.1001/archsurg.136.1.25
3. Zhou L, Rui JA, Zhou WX, Wang SB, Chen SG, Qu Q. Edmondson-Steiner grade: a crucial predictor of recurrence and survival in hepatocellular carcinoma without microvascular invasio. *Pathol Res Pract*. 2017;213:824–830. doi:10.1016/j.prp.2017.03.002
4. Granata V, Fusco R, Filice S, et al. The current role and future prospectives of functional parameters by diffusion weighted imaging in the assessment of histologic grade of HCC. *Infect Agent Cancer*. 2018;13:23. doi:10.1186/s13027-018-0194-5
5. Moriya T, Saito K, Tajima Y, et al. 3D analysis of apparent diffusion coefficient histograms in hepatocellular carcinoma: correlation with histological grade. *Cancer Imaging*. 2017;17:1. doi:10.1186/s40644-016-0103-3
6. Amano S, Ebara M, Yajima T, et al. Assessment of cancer cell differentiation in small hepatocellular carcinoma by computed tomography and magnetic resonance imaging. *J Gastroenterol Hepatol*. 2003;18:273–279. doi:10.1046/j.1440-1746.2003.02957.x
7. Muhi A, Ichikawa T, Motosugi U, et al. High-b-value diffusion-weighted MR imaging of hepatocellular lesions: estimation of grade of malignancy of hepatocellular carcinoma. *J Magn Reson Imaging*. 2009;30:1005–1011. doi:10.1002/jmri.21931
8. Yang C, Wang H, Sheng R, Ji Y, Rao S, Zeng M. Microvascular invasion in hepatocellular carcinoma: is it predictable with a new, preoperative application of diffusion-weighted imaging? *Clin Imaging*. 2017;41:101–105. doi:10.1016/j.clinimag.2016.10.004
9. Nakanishi M, Chuma M, Hige S, et al. Relationship between diffusion-weighted magnetic resonance imaging and histological tumor grading of hepatocellular carcinoma. *Ann Surg Oncol*. 2012;19:1302–1309. doi:10.1245/s10434-011-2066-8
10. Le Bihan D. Apparent diffusion coefficient and beyond: what diffusion MR imaging can tell us about tissue structure. *Radiology*. 2013;268:318–322. doi:10.1148/radiol.13130420
11. Lu H, Jensen JH, Ramani A, Helpern JA. Three-dimensional characterization of non-gaussian water diffusion in humans using diffusion kurtosis imaging. *NMR Biomed*. 2006;19:236–247. doi:10.1002/nbm.1020
12. Shaw CB, Jensen JH, Deardorff RL, Spampinato MV, Helpern JA. Comparison of diffusion metrics obtained at 1.5T and 3T in human brain with diffusional kurtosis imaging. *J Magn Reson Imaging*. 2017;45(3):673–680. doi:10.1002/jmri.25380
13. Rea DJ, Munoz-Juarez M, Farnell MB, et al. Major hepatic resection for hilar cholangiocarcinoma: analysis of 46 patients. *Arch Surg*. 2004;139(5):523–525. doi:10.1001/archsurg.139.5.514
14. Shirota N, Saito K, Sugimoto K, Takara K, Moriyasu F, Tokuuye K. Intravoxel incoherent motion MRI as a biomarker of sorafenib treatment for advanced hepatocellular carcinoma: a pilot study. *Cancer Imaging*. 2016;16:1.
15. Dai Y, Yao Q, Wu G, et al. Characterization of clear cell renal cell carcinoma with diffusion kurtosis imaging: correlation between diffusion kurtosis parameters and tumor cellularity. *NMR Biomed*. 2016;29:873. doi:10.1002/nbm.3535
16. Barbieri S, Bronnimann M, Boxler S, Vermathen P, Thoeny HC. Differentiation of prostate cancer lesions with high and with low Gleason score by diffusion-weighted MRI. *Eur Radiol*. 2017;27(4):1547–1555. doi:10.1007/s00330-016-4449-5
17. Winfield JM, Orton MR, Collins DJ, et al. Separation of type and grade in cervical tumours using non-mono-exponential models of diffusion-weighted MRI. *Eur Radiol*. 2017;27(2):627–636. doi:10.1007/s00330-016-4417-0
18. Collier Q, Veraart J, Jeurissen B, et al. Diffusion kurtosis imaging with free water elimination: a bayesian estimation approach. *Magn Reson Med*. 2018;80:802–813. doi:10.1002/mrm.27075
19. Rosenkrantz AB, Padhani AR, Chenevert TL, et al. Body diffusion kurtosis imaging: basic principles, applications, and considerations for clinical practice. *J Magn Reson Imaging*. 2015;42:1190–1202. doi:10.1002/jmri.24985
20. Wang WT, Yang L, Yang ZX, et al. Assessment of microvascular invasion of hepatocellular carcinoma with diffusion kurtosis imaging. *Radiology*. 2018;286:571–580. doi:10.1148/radiol.2017170515
21. Cao L, Chen J, Duan T, et al. Diffusion kurtosis imaging (DKI) of hepatocellular carcinoma: correlation with microvascular invasion and histologic grade. *Quant Imaging Med Surg*. 2019;9:590–602. doi:10.21037/qims.2019.02.14
22. European Association for the Study of the Liver. Electronic address eee, European Association for the Study of the L. EASL clinical practice guidelines: management of hepatocellular carcinoma. *J Hepatol*. 2018;69:182–236. doi:10.1016/j.jhep.2018.03.019
23. Woo S, Lee JM, Yoon JH, Joo I, Han JK, Choi BI. Intravoxel incoherent motion diffusion-weighted MR imaging of hepatocellular carcinoma: correlation with enhancement degree and histologic grade. *Radiology*. 2014;270:758. doi:10.1148/radiol.13130444
24. Kazmierczak PM, Theisen D, Thierfelder KM, et al. Improved detection of hypervascular liver lesions with CAIPIRINHA-Dixon-TWIST-volume-interpolated breath-hold examination. *Invest Radiol*. 2015;50:153. doi:10.1097/RLI.0000000000000118
25. Steinmann C, Christensen AS, Jensen JH. Interface of the polarizable continuum model of solvation with semi-empirical methods in the GAMESS program. *PLoS One*. 2013;8:e67725. doi:10.1371/journal.pone.0067725

26. Wile GE, Leyendecker JR. Magnetic resonance imaging of the liver: sequence optimization and artifacts. *Magn Reson Imaging Clin N Am*. 2010;18:525–547. doi:10.1016/j.mric.2010.07.010
27. Yan C, Xu J, Xiong W, et al. Use of intravoxel incoherent motion diffusion-weighted MR imaging for assessment of treatment response to invasive fungal infection in the lung. *Eur Radiol*. 2017;27:212. doi:10.1007/s00330-016-4380-9
28. Jensen JH, Helpern JA. MRI quantification of non-Gaussian water diffusion by kurtosis analysis. *NMR Biomed*. 2010;23(7):698–710. doi:10.1002/nbm.1518
29. Rosenkrantz AB, Sigmund EE, Winnick A, et al. Assessment of hepatocellular carcinoma using apparent diffusion coefficient and diffusion kurtosis indices: preliminary experience in fresh liver explants. *Magn Reson Imaging*. 2012;30:1534–1540. doi:10.1016/j.mri.2012.04.020
30. Yuan ZG, Wang ZY, Xia MY, et al. Comparison of diffusion kurtosis imaging versus diffusion weighted imaging in predicting the recurrence of early stage single nodules of hepatocellular carcinoma treated by radiofrequency ablation. *Cancer Imaging*. 2019;19:30. doi:10.1186/s40644-019-0213-9
31. An C, Kim DW, Park YN, Chung YE, Rhee H, Kim MJ. Single hepatocellular carcinoma: preoperative MR imaging to predict early recurrence after curative resection. *Radiology*. 2015;276:433–443. doi:10.1148/radiol.15142394
32. Edmondson HA, Steiner PE. Primary carcinoma of the liver: a study of 100 cases among 48,900 necropsies. *Cancer*. 1954;7:462–503. doi:10.1002/1097-0142(195405)7:3<462::AID-CNCR2820070308>3.0.CO;2-E
33. Tang Y, Wang H, Ma L, et al. Diffusion-weighted imaging of hepatocellular carcinomas: a retrospective analysis of correlation between apparent diffusion coefficients and histological grade. *Abdom Radiol (NY)*. 2016;41:1539–1545. doi:10.1007/s00261-016-0715-x
34. Jiang T, Xu JH, Zou Y, et al. Diffusion-weighted imaging (DWI) of hepatocellular carcinomas: a retrospective analysis of the correlation between qualitative and quantitative DWI and tumour grade. *Clin Radiol*. 2017;72:465–472. doi:10.1016/j.crad.2016.12.017
35. Yoshimaru D, Miyati T, Suzuki Y, et al. Diffusion kurtosis imaging with the breath-hold technique for staging hepatic fibrosis: a preliminary study. *Magn Reson Imaging*. 2018;47:33–38. doi:10.1016/j.mri.2017.11.001
36. Yang L, Rao S, Wang W, et al. Staging liver fibrosis with DWI: is there an added value for diffusion kurtosis imaging? *Eur Radiol*. 2018;28:3041–3049. doi:10.1007/s00330-017-5245-6
37. Min JH, Kim YK, Lim S, Jeong WK, Choi D, Lee WJ. Prediction of microvascular invasion of hepatocellular carcinomas with gadoxetic acid-enhanced MR imaging: impact of intra-tumoral fat detected on chemical-shift images. *Eur J Radiol*. 2015;84:1036–1043. doi:10.1016/j.ejrad.2015.03.002
38. Goshima S, Kanematsu M, Noda Y, Kondo H, Watanabe H, Bae KT. Diffusion kurtosis imaging to assess response to treatment in hypervascular hepatocellular carcinoma. *AJR Am J Roentgenol*. 2015;204:W543–W549. doi:10.2214/AJR.14.13235
39. Yoon JH, Lee JM, Yu MH, Kiefer B, Han JK, Choi BI. Evaluation of hepatic focal lesions using diffusion-weighted MR imaging: comparison of apparent diffusion coefficient and intravoxel incoherent motion-derived parameters. *J Magn Reson Imaging*. 2014;39:276–285. doi:10.1002/jmri.24158
40. Taouli B, Koh DM. Diffusion-weighted MR imaging of the liver. *Radiology*. 2010;254:47–66. doi:10.1148/radiol.09090021
41. Chandarana H, Taouli B. Diffusion and perfusion imaging of the liver. *Eur J Radiol*. 2010;76:348–358. doi:10.1016/j.ejrad.2010.03.016
42. Li H, Ma J, Zhang X. Diffusion tensor imaging of spinocerebellar ataxia type 12. *Med Sci Monit*. 2014;20:1783–1791. doi:10.12659/MSM.891104
43. White NS, Dale AM. Distinct effects of nuclear volume fraction and cell diameter on high b-value diffusion MRI contrast in tumors. *Magn Reson Med*. 2014;72:1435–1443. doi:10.1002/mrm.25039
44. Poot DH, den Dekker AJ, Achten E, Verhoye M, Sijbers J. Optimal experimental design for diffusion kurtosis imaging. *IEEE Trans Med Imaging*. 2017;45(3):819. doi:10.1109/TMI.2009.2037915
45. Glenn GR, Helpern JA, Tabesh A, Jensen JH. Quantitative assessment of diffusional kurtosis anisotropy. *NMR Biomed*. 2015;28(4):448–459. doi:10.1002/nbm.3271
46. Jensen JH, Helpern JA, Ramani A, Lu H, Kaczynski K. Diffusional kurtosis imaging: the quantification of non-gaussian water diffusion by means of magnetic resonance imaging. *Magn Reson Med*. 2005;53:1432–1440. doi:10.1002/mrm.20508